ARCHIVIO ISTITUZIONALE
DELLA RICERCA

Alma Mater Studiorum Università di Bologna
Archivio istituzionale della ricerca

A numerical procedure for the force-displacement description of out-of-plane collapse mechanisms in masonry structures

This is the final peer-reviewed author's accepted manuscript (postprint) of the following publication:

Published Version:
D'Altri A.M., de Miranda S., Milani G., Castellazzi G. (2020). A numerical procedure for the force-displacement description of out-of-plane collapse mechanisms in masonry structures. COMPUTERS & STRUCTURES, 233(June 2020), 1-16 [10.1016/j.compstruc.2020.106234].

Availability:
This version is available at: https://hdl.handle.net/11585/754650 since: 2020-04-08

Published:

DOI: http://doi.org/10.1016/j.compstruc.2020.106234

Terms of use:

Some rights reserved. The terms and conditions for the reuse of this version of the manuscript are specified in the publishing policy. For all terms of use and more information see the publisher's website.

This item was downloaded from IRIS Università di Bologna (https://cris.unibo.it/).
When citing, please refer to the published version.

(Article begins on next page)

17 September 2024

This is the final peer-reviewed accepted manuscript of:

Antonio Maria D'Altri, Stefano de Miranda, Gabriele Milani, Giovanni Castellazzi, *A numerical procedure for the force-displacement description of out-of-plane collapse mechanisms in masonry structures*, Computers & Structures, Volume 233, 2020, 106234,

ISSN 0045-7949

The final published version is available online at: https://doi.org/10.1016/j.compstruc.2020.106234

© 2020. This manuscript version is made available under the Creative Commons Attribution-NonCommercial-NoDerivs (CC BY-NC-ND) 4.0 International License

(http://creativecommons.org/licenses/by-nc-nd/4.0/)

A numerical procedure for the force-displacement description of out-of-plane collapse mechanisms in masonry structures

Antonio Maria D'Altri[1], Stefano de Miranda[1]*, Gabriele Milani[2], Giovanni Castellazzi[1]

[1] Department of Civil, Chemical, Environmental, and Materials Engineering (DICAM), University of Bologna, Viale del Risorgimento 2, Bologna 40136, Italy

[2] Department of Architecture, Built Environment and Construction Engineering, Technical University of Milan, Piazza Leonardo Da Vinci, Milan 20133, Italy

*corresponding author

ABSTRACT

In this paper, a novel numerical procedure is proposed for the force-displacement description of out-of-plane collapse in masonry structures. The numerical procedure herein proposed represents one first attempt to couple limit analysis-based solutions to displacement-based evolutive analysis strategies. Limit-analysis based solutions are considered trustworthy to investigate collapse mechanisms in masonry structures, even though they cannot be used in displacement-based seismic assessment procedures (e.g. pushover analysis), while displacement-based evolutive analysis strategies (e.g. block-based and anisotropic continuum approaches), which can undertake this last task, are typically computationally demanding and their mechanical characterization is often very challenging. In this research, a genetic algorithm NURBS-based adaptive homogenized upper bound limit analysis is firstly adopted to compute the collapse mechanism that the structure (of any geometrical complexity) experiences for a given loading condition. Then, the 3D geometry of the collapse mechanism is imported in incremental-iterative step-by-step evolutive analysis frameworks to perform pushover analysis. In particular, two numerical modelling approaches are conceived to this aim, both lumping all the mechanical nonlinearities into tight zones located in correspondence of the cracks defined in the collapse mechanism previously computed. The first one uses 3D plastic damaging strips governed by a standard nonlinear continuum constitutive law. The second approach adopts non-standard zero-thickness contact-based interfaces governed by a cohesive-frictional contact behaviour previously developed by the authors for the brick-to-brick mechanical interaction. A number of meaningful structural examples show the effectiveness of the numerical procedure proposed. Pushover curves obtained through different modelling strategies are also critically compared.

Keywords: Unreinforced masonry; Limit analysis; Collapse mechanisms; Out-of-plane behaviour

1 Introduction

The relevance that European citizens attach to heritage structures proves their high societal value. One of the main actions which threaten the conservation of heritage structures is represented by seismic actions, especially in southern Europe [1]. Indeed, past and recent earthquakes clearly highlighted the high seismic vulnerability of historical buildings [2], which typically show cracks and partial (or even full) collapses.

The evaluation of the seismic behaviour of a historical building is a difficult task, given the complex geometries which characterize heritage structures and the complex mechanics of masonry. Several numerical modelling strategies have been developed in the last decades to deal with collapse analysis of masonry structures [3]. The collapse or near-collapse response of masonry structures can be studied following two main analysis approaches: (i) limit analysis-based solutions and (ii) incremental-iterative evolutive analyses.

On the one hand, limit-analysis based solutions are typically based on the theoretical background proposed by Heyman [4], who firstly applied limit theorems of plasticity to masonry structures. Starting from this pioneering work [4], many researchers developed limit-analysis based numerical approaches for masonry structure using both the static theorem (lower bound limit analysis [5, 6, 7, 8]) and the kinematic theorem (upper bound limit analysis [9, 10, 11]). Technically, limit analysis procedures which uses finite elements (FEs) are typically based on the upper bound theorem, and for cohesive-frictional materials (e.g. masonry) the solution appears particularly reliable when dissipation relies on interfaces between contiguous elements, following the idea proposed in [12].

Limit analysis-based solutions are considered trustworthy to investigate collapse mechanisms and the ultimate load in masonry structures [3]. Nevertheless, in these analysis approaches no information is available on the ultimate displacement and/or post-peak response. This aspect appears essential in extensively employed displacement-based seismic assessment methods (based on pushover analysis). Indeed, these assessment methods should be preferred rather than force-based assessment methods as stated in [13] for masonry structures.

On the other hand, incremental-iterative evolutive analysis procedures investigate step-by-step the evolution of the equilibrium conditions of a structure subjected to certain actions. The loading and the structural response are divided into a sequence of increments, and iterations are conducted to reach equilibrium within each increment. These procedures can account for mechanical and geometric nonlinearities, allowing the description of the force-displacement response (pushover curve) of the structure (and, so, they are employable in displacement-based methods).

Overlooking macroelement models which are typically limited to ordinary masonry buildings (and generally non-applicable to monumental structures), incremental-iterative evolutive analysis can be used in (i) block-based and (ii) continuum models. In block-based models, masonry is modelled in a block-by-block fashion accounting for the actual masonry texture [14]. The block behaviour can be considered rigid or deformable, whereas their interaction can be mechanically represented through various suitable formulations (i.e. interface element-based [15, 16, 17, 18], contact-based [19, 20], textured continuum-based [21, 22] and extended finite element-based approaches [23]). The main issue of these models lies in their huge computational demand, being their application to non-periodic masonry [24] and to full-scale monumental masonry structure still unlikely.

In continuum models, masonry is modelled as a continuum deformable material, without distinction between bricks and mortar layers. The constitutive law adopted for the material can be defined either through (i) direct approaches [25, 26, 27, 28, 29], i.e. by means of anisotropic constitutive laws calibrated, for example, on experimental tests [30], or through (ii) homogenization procedures and multi-scale approaches [31, 32, 33], where the constitutive law of the material is deduced from a homogenization process which relates the structural-scale model to a material-scale model of a representative volume element (RVE) of the structure. However, many of these approaches are often computationally expensive, and their practical application is typically limited to panel-scale structures. Other computationally reduced simplistic continuum approaches, although not entirely consistent with the anisotropic nature of masonry (e.g. smeared crack [34], isotropic damage [35] and plastic-damage [36, 37] models), could be followed when dealing with large-scale monumental masonry structures. However, the pushover curves obtained with these approaches should be carefully considered, especially in the post-peak response, as the predicted cracks and damage are typically smeared on the structure and the development of collapse mechanism is generally not entirely clear or physically meaningful [3].

It has to be pointed out that force-displacement responses of masonry structures could be also analytically defined (see for example Godio & Beyer [38, 39]). Although employable in standard engineering practice, analytical approaches are typically restricted to standard and simple geometries, while the geometrical complexity is a peculiar feature of heritage structures.

In this paper, a novel numerical procedure is proposed for the force-displacement description of out-of-plane collapse in masonry structures. The numerical procedure herein proposed represents one first attempt to couple

limit analysis-based solutions to incremental-iterative evolutive analysis strategies. Indeed, the idea at the base of this procedure, although simple, is original.

Adaptive NURBS-based limit analysis is firstly adopted to compute the collapse mechanism that the structure (of any geometrical complexity) experiences for a given loading condition. This recently proposed approach [40, 41, 42] utilizes a meta-heuristic framework (genetic algorithm) and a homogenized upper bound limit analysis formulation.

Then, the 3D geometry of the collapse mechanism is imported in incremental-iterative step-by-step evolutive analysis frameworks to perform pushover analysis. Two numerical modelling approaches, which lump all the mechanical nonlinearities into tight zones located in correspondence of the cracks defined in the collapse mechanism previously computed, are conceived to this aim. The first one uses 3D plastic damaging strips governed by a nonlinear continuum constitutive law (i.e. the so-called concrete damaged plasticity (CDP) model [43] implemented in the commercial FE software Abaqus [44]). The second approach adopts non-standard zero-thickness contact-based interfaces governed by a cohesive-frictional contact behaviour previously developed by the authors in [45] for the brick-to-brick mechanical interaction. A number of meaningful structural examples are used to test the efficiency of the numerical analysis procedure proposed.

The paper is organized as follows. Section 2 describes the numerical analysis procedure proposed for the force-displacement description of collapse in masonry structures. Section 3 briefly recalls the adaptive NURBS-based limit analysis approach. Section 4 briefly recalls the two incremental-iterative step-by-step evolutive analysis frameworks utilized in this research, i.e. plastic damaging strips (in the following named as CDP) and contact-based interfaces (in the following named as CONT). Section 5 shows some parametric analyses on a simple benchmark. Section 6 collects the results of structural examples, where the pushover curves obtained through different modelling strategies are also critically compared. Finally, Section 7 highlights the conclusions of this research work.

2 Analysis procedure proposed

The main steps of the analysis procedure proposed in this paper for the force-displacement description of collapse mechanisms in masonry structures are shown in Fig. 1.

Firstly, the real structure is idealized into a 3D solid NURBS-based geometry (Fig. 1). This standard operation can be manually conducted on well-known commercial or open source computer-aided design (CAD) software packages, which typically use special approximating base function (i.e. NURBS) for the 3D modelling [40]. Of course, preliminary knowledge acquisition phases, which consist in archival historical background analyses and material-geometrical surveys, appear essential when dealing with heritage structures [46].

Then, loading conditions are applied to the structure to simulate, for example, the seismic action (Fig. 1), see [41]. Consequently, adaptive NURBS-based upper bound limit analysis [40, 41, 42] (briefly recalled in Section 3) is carried out to investigate the collapse mechanism (Fig. 1) and the collapse load multiplier of the structure.

The geometry of the collapse mechanism is automatically imported into incremental-iterative step-by-step evolutive analysis frameworks (Fig. 1) to perform pushover analysis (see Section 4). In this research, plastic damaging strips (CDP) and contact-based interfaces (CONT), which lump all the nonlinearities into tight zones located in correspondence of the cracks defined in the collapse mechanism, are used to this aim. Particularly, the CDP approach adopts finite-thickness 3D strips characterized by a plastic damage nonlinear behaviour (Section 4.1), while the CONT approach utilizes zero-thickness contact-based cohesive-frictional interfaces (Section 4.2).

Consequently, pushover curves which describe the force-displacement evolution of collapse mechanisms are obtained and they can be used in displacement-based seismic assessment methods [13]. Moreover, a further assessment of the reliability of the approach can be achieved by comparing the collapse load multiplier obtained by means of adaptive limit analysis and the peak load of the pushover curve.

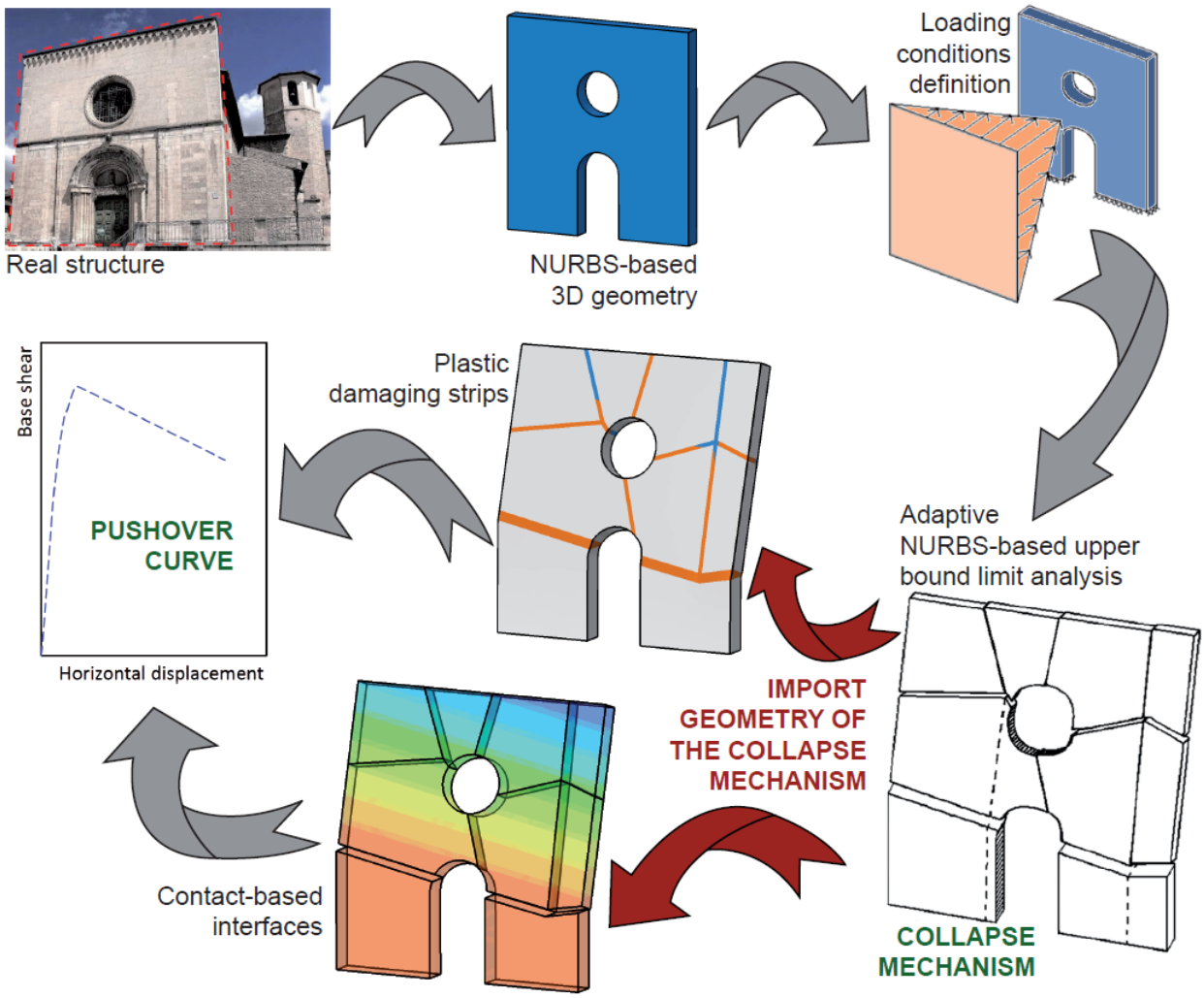

Fig. 1 – Analysis procedure proposed.

3 Adaptive NURBS-based limit analysis

In this section, the main features of the adaptive NURBS-based limit analysis, originally developed in [40] for masonry vaults and in [42, 41] for heritage structures, are briefly recalled.

3.1 NURBS geometric description

Any 3D solid geometry representing a masonry structure can be modelled within any free form 3D modeler using NURBS surfaces and a rigid block assembly can be defined on it, as sketched in Fig. 2. For instance, a Rhinoceros [47] 3D geometric model can be used, which interfaces to MATLAB® for the creation of a coarse NURBS mesh.

The proposed approach begins with a representation of the geometry of the structure by means of NURBS surfaces in a CAD environment. NURBS surfaces are parametric surfaces in the 3D Euclidean space defined by a bidirectional net of control points, an equal number of weights, and a rational basis function built on B-spline basis functions [48]. By exploiting the properties of NURBS functions, a mesh of the given geometry, which still provides an exact representation of the structure, can be obtained. Therefore, a given masonry structure with any geometry can be represented by very few NURBS parametric elements. Each NURBS element of the mesh is idealized as a rigid body (Fig. 3a-c). For NURBS geometries, B-spline basis functions

are piecewise polynomial functions defined by a knot-vector which is not uniform (i.e. knot-points are not equidistant). Starting from a knot-vector $\Xi = [\xi_1, \xi_2, \dots \xi_{n+p+1}]$, where p and n denote respectively the polynomial order and the total number of basis functions, a given set of weights $w_i \in \mathbb{R}$ and the i-th B-spline basis function ($N_{i,p}$), the NURBS basis function $R_{i,p}$ is defined as follows:

$$R_{i,p}(\xi) = \frac{N_{i,p}(\xi) w_i}{\sum_{j=1}^{n} N_{j,p}(\xi) w_j} \quad (1)$$

Given a bidirectional net of control points $\mathbf{B}_{i,j}$, a set of weights $w_{i,j}$ and two separate knot-vectors in both u and v directions, a NURBS surface of degree p in the u-direction and q in the v-direction is defined as:

$$S(u,v) = \sum_{i=0}^{n} \sum_{j=0}^{m} R_{i,j}(u,v) \mathbf{B}_{i,j} \quad (2)$$

More details on the theory of NURBS applied to limit analysis are provided in [40], where the reader is referred for further details. Here, it is only worth mentioning that such surfaces are commonly used in computational graphics, so they can be found in all CAD-based software (e.g. AutoCAD, Rhinoceros and SolidWorks). The main advantage is the possibility of dealing with complex geometries, i.e. curved geometries of any shape and openings, with few surfaces. Therefore, an accurate representation of the three-dimensional geometry can be realized with negligible computational efforts. Moreover, a NURBS model requires less computational memory in comparison with traditional three-dimensional CAD models, turning out to be much easier to build, handle and modify.

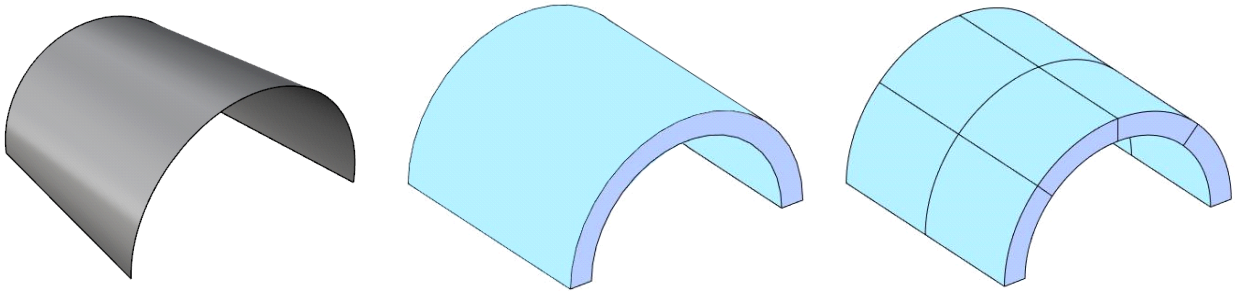

(a) (b) (c)

Fig. 2 - From Rhinoceros to MATLAB: (a) NURBS surface in Rhinoceros, (b) NURBS model in MATLAB and (c) mesh of NURBS element.

The obtained model can be automatically imported into the structural analysis program (e.g. MATLAB®) through the IGES (Initial Graphics Exchange Specification) standard format [49]. Thickness and offset properties can be assigned to each surface. NURBS properties can be manipulated to define a NURBS mesh of the masonry mid-surface, in which each element is a NURBS surface itself. More specifically, assuming a certain NURBS surface indicated as $S(u,v)$, a certain point on the parametric domain is described by its parametric coordinates (u_0, v_0). The corresponding point in the three-dimensional Euclidean space is obtained as $S(u_0, v_0)$; therefore, if a curve is defined on the parametric domain the corresponding three-dimensional curve belonging to the NURBS surfaces can be identified. Similarly, isocurves, or isoparametric curves, can be defined on the surface by fixing one parameter in the parameter space and letting the other vary: by fixing $u = u_0$ the isoparametric curve $s(u_0, v)$ is defined on the surface S, whereas by fixing $v = v_0$ the isocurve $s(u, v_0)$ is obtained. Therefore, a NURBS mesh can be defined through a lattice of isocurves, which are obtained merely by subdividing the parametric domain with horizontal and vertical lines. By modifying the NURBS lines in the parametric domain (for example, by changing slopes or parametric coordinates of

intersection points), adjustment of the NURBS mesh can be performed and elements of different shapes can be obtained.

3.2 Upper Bound NURBS limit analysis

Starting from the obtained rigid bodies assembly, an upper bound limit analysis problem with very few optimization variables has been derived in [40], assuming dissipation allowed only along element edges. The same approach is utilized here. In particular, given an initial NURBS mesh, each element is idealized as a rigid body and its kinematics is thus determined by the six generalized velocity components $\mathbf{u}^i = \left[u_x^i, u_y^i, u_z^i, \Phi_x^i, \Phi_y^i, \Phi_z^i\right]$ of its center of mass, expressed in a global reference system $Oxyz$. A configuration of dead loads $\mathbf{f_D}$ and live loads $\mathbf{f_L}$ is defined. The plastic dissipation is allowed only along element edges. In the evaluation of plastic dissipation energy, integrals are numerically evaluated by subdividing each interface in a series of points P_j and applying on each one an associated flow rule. According to the hypotheses of the limit analysis theorems, rigid plastic behaviour is assigned to masonry material. Therefore, the plastic dissipation at each interface is linear and, if we define as $\mathbf{p}$ the vector of all plastic multipliers at the interface points, the total dissipation can be readily calculated. A local reference system $(\mathbf{n}, \mathbf{s}, \mathbf{t})$ is defined at each point, where $\mathbf{n}$ is the unit vector normal to the interface, $\mathbf{s}$ is the tangential unit vector in the longitudinal direction and $\mathbf{t}$ is the tangential unit vector in the transversal direction, as sketched in Fig. 3(d). In this way, elements interfaces assume the meaning of possible fracture lines.

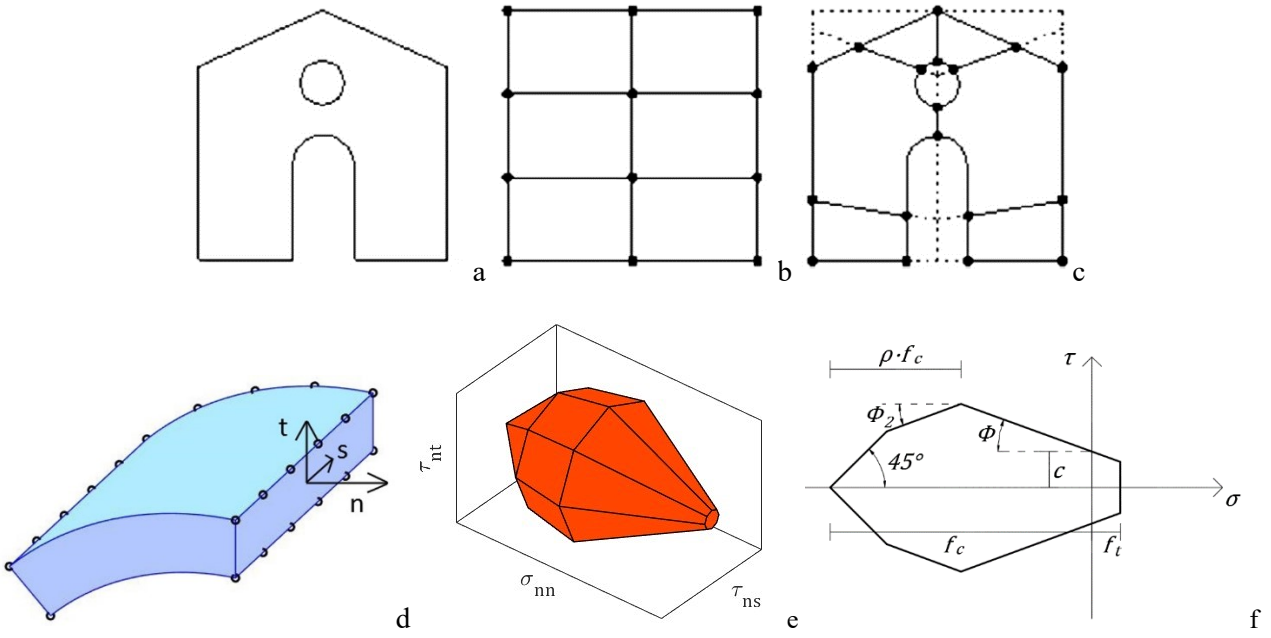

Fig. 3 – Adaptive NURBS-based limit analysis: (a) example of NURBS model, (b) initial subdivision, (c) final GA-modified subdivision, (d) planar interface between NURBS elements, (e) 3D linearized failure surface and (f) 2D section.

A homogenized three-dimensional failure surface is adopted, which includes tension cut-off, Mohr-Coulomb frictional behaviour and a linear cap in compression; an example of 3D failure surfaces with the nomenclature of the parameters involved is shown in Fig. 3(e-f). The adoption of suitable homogenization techniques is preferred in comparison with traditional isotropic no-tension material, as recommended for instance by Milani and co-workers [50, 51, 52]. It is clear that the traditional Heyman model for masonry can be represented by setting zero value in tension and with high values of compression strength and cohesion.

The NURBS-based upper bound limit analysis procedure is implemented as a linear programming problem that includes: (a) geometric and compatibility constraints, (b) non-negativity of plastic multipliers and (c)

normalization condition of the work done by live loads. The resultant linear programming problem is therefor quite standard, characterized by very few optimization variables and can be written as follows:

$$\begin{aligned} &\text{Min} && \lambda = \frac{\mathbf{c}\cdot\mathbf{p} - \mathbf{f_D}\cdot\mathbf{u}}{\mathbf{f_L}\cdot\mathbf{u}} \\ &\text{subjected to} && \mathbf{A}\cdot\mathbf{u} - \mathbf{C}\cdot\mathbf{p} = 0 \quad \text{(a)} \\ & && \mathbf{p} \geq 0 \quad \text{(b)} \\ & && \mathbf{f_L}\cdot\mathbf{u} = 1 \quad \text{(c)} \end{aligned} \tag{3}$$

Where, apart the symbols already introduced, other symbols have the following meaning:

- **A** and **C** are assembled rectangular matrices of geometric coefficients entering in the geometric and compatibility constraints;
- **p** and **u** are respectively the assembled vectors of plastic multiplier rates and elements generalized velocities;
- **c**, $\mathbf{f_D}$ and $\mathbf{f_L}$ are vectors of coefficients for the internal dissipated power, that dissipated by external loads λ independent and that dissipated by external loads λ dependent.

The solution is found through the MATLAB toolbox for optimization over symmetric cones SeDuMi (Self-Dual-Minimization [53]).

Due to the very limited number of rigid elements used, the quality of the collapse load so found depends on the shape and position of the interfaces, where dissipation is allowed. Mesh adjustments are therefore needed, and a specific Genetic Algorithm is adopted, as described in what follows.

3.3 Genetic algorithm

Mesh adjustments can be carried out by adopting a simple meta-heuristic approach of mesh adjustment, e.g. genetic algorithm (GA) [54]. In this way, each individual which composes the population is constituted of a mesh. Typically, each iteration requires the solution of a linear programming problem for each individual.

The objective function of the genetic algorithm is represented by the internal power dissipated minus the power expended by the loads independent upon the load multiplier. Considering the so-called normalization condition, which equates to the unitary value the power expended by loads dependent upon the load multiplier assumed equal to one, the objective function turns out to be equal to the load multiplier. Within the upper bound theorem of limit analysis, such quantity must be minimized when subjected to equality and inequality constraints.

Given the very reduced number of NURBS elements used in the discretization, the computational demand needed in each iteration appears practically negligible. After each generation, the GA typically works on a population of potential failure mechanisms, applying the principle of survival of the fittest to produce better and better approximations to a solution [54], i.e. moving the interfaces towards the actual failure mechanism. At each generation, a new set of approximations is generated by choosing individuals according to their level of fitness (i.e. the value of the collapse load) in the problem domain and breeding them together using operators borrowed from natural genetics (crossover, mutation and reproduction). This process typically leads rapidly to the evolution of populations of individuals that are better suited to their environment than the individuals that they were created from, with a very accurate estimation of both collapse loads and failure mechanisms after few generations. Accordingly, even if the mesh is made of very few elements (which therefore require a

practically negligible computational time to have the assessment of collapse load), accurate load multipliers and failure mechanisms can be obtained.

4 Force-displacement description of collapse mechanisms

Two numerical modelling approaches (CDP and CONT, see Fig. 4) are used to obtain the force-displacement description of collapse mechanisms (previously computed through adaptive limit analysis). These approaches need as input the geometry of the collapse mechanism and give as output the pushover curve (Fig. 4).

In the first approach with plastic damaging strips (Fig. 4, top), once the geometry of the collapse mechanism is imported (the geometry can be automatically imported into the software Abaqus [44] by means of a MATLAB® .fig file generated from adaptive limit analysis), manual partitioning of the geometry is needed to define the finite thickness of the strips. Some suggestions about the thickness of the strip to adopt in the simulations are given in Section 5. The material of the strips (CDP) is then distinguished from the material of the remaining structure (assumed linear elastic). A brief description of the plastic-damage constitutive law adopted for the strips is given in Section 4.1. After standard meshing operations and loading condition definitions, an incremental-iterative evolutive analysis is conducted by means of a quasi-static implicit dynamic algorithm [44] to investigate the collapse behaviour of the structure. Accordingly, the potential softening behaviour can be described in the structural response.

In the second approach with contact-based interfaces (Fig. 4, bottom), the geometry of the collapse mechanism is imported analogously to the previous approach. No manual partitioning of the geometry is here requested as zero-thickness interfaces are adopted. A fully automatic contact detection algorithm [44] is used to define the interactions between the geometrical portions (which defines the collapse mechanism). Standard meshing operations are carried out on the geometrical portions. In general, conforming mesh are considered on the domain of each geometrical portion, i.e. the mesh of each geometrical portion is not conforming with the adjacent ones. Node-to-surface contact definitions are implemented to compute the interactions between adjacent geometrical portions. Linear elastic isotropic material behaviour is supposed for the 3D solid FEs, while a cohesive-frictional contact definition is adopted for the zero-thickness interfaces (briefly described in Section 4.2).

Geometric nonlinearity is accounted for in the incremental-iterative evolutive analyses, as large-displacement effects evidently arise in the force-displacement description of collapse mechanisms. A quasi-static direct-integration dynamic analysis algorithm has been adopted to compute the solution up to the collapse of the structure. This algorithm permits to simulate quasi-static responses in which inertia effects are exclusively introduced to regularize unstable behaviours. The Authors experienced a better performance of this algorithm, specifically in terms of convergence, with respect to more common arc length procedures.

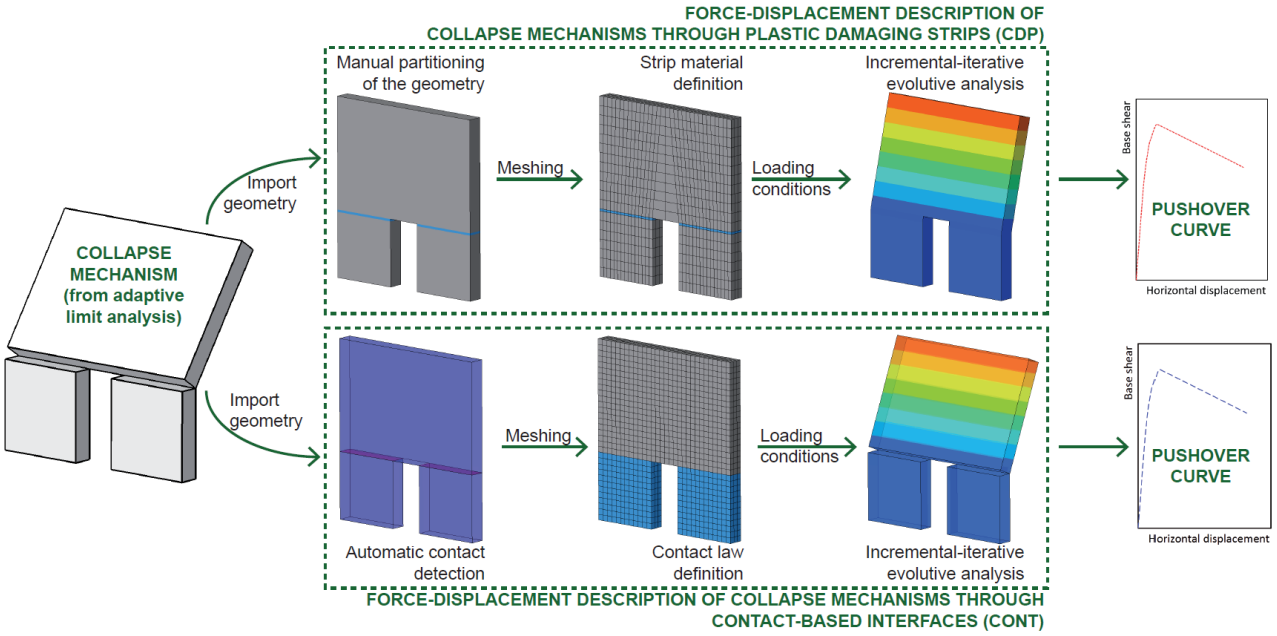

Fig. 4 – Force-displacement description of collapse mechanisms through plastic damaging strips (CDP) and contact-based interfaces (CONT).

4.1 Plastic-damage constitutive law

The continuum plastic-damage constitutive model, originally developed in [43] and herein utilized for the nonlinear strips, is characterized by a yielding function with multiple-hardening variables and two independent scalar damage variables, one for the tensile damage ($0 \leq d_t < 1$) and the other for compressive damage ($0 \leq d_c < 1$). The stress-strain relations in uniaxial tension, σ_t, and compression, σ_c, are:

$$\sigma_t = (1 - d_t)E\left(\varepsilon_t - \varepsilon_t^p\right), \qquad \sigma_c = (1 - d_c)E\left(\varepsilon_c - \varepsilon_c^p\right), \tag{4}$$

where E is the initial Young's modulus of the material, ε_t and ε_c are the uniaxial tensile and compressive strains, and ε_t^p and ε_c^p are the uniaxial tensile and compressive plastic strains). A multiple-hardening Drucker-Prager type surface, which is eventually smoothed towards a Mohr-Coulomb criterion type through the shape constant ρ, is adopted as yield surface in the plastic-damage constitutive law.

Being the model formulated in the context of nonassociated plasticity [43], the plastic potential is defined by the dilatancy angle ψ, generally assumed equal to 10° for masonry [36], as well as by a smoothing parameter ϵ usually assumed equal to 0.1 [36]. In addition, the strength domain is specified by the ratio f_{b0}/f_{c0} between the biaxial f_{b0} and uniaxial f_{c0} initial compressive strengths, typically assumed equal to 1.16 [36], and by the shape constant ρ, normally assumed equal to 2/3 [43]. The general parameters for the plastic damaging behaviour are collected in Table 1. It has to be pointed out that in this constitutive model the shear behaviour is not directly defined, whereas it depends on both the tensile and compressive uniaxial responses. Linear softening is supposed in both tensile and compressive responses after reaching the tensile (f_t) and compressive (f_c) uniaxial strengths.

Finally, it has to be pointed out that the shear behaviour in this plastic-damage constitutive law is indirectly described by specifying the tensile and compressive uniaxial behaviours. Although the ultimate shear depends on the level of confinement, a direct control of shear is not pursuable in CDP strips.

Table 1. General parameters for the plastic damaging behaviour.

ϵ	ψ	f_{b0}/f_{c0}	ρ
0.1	10°	1.16	2/3

4.2 Contact-based cohesive-frictional interfaces

The zero-thickness contact-based interfaces with linear degradation of cohesion utilized in this research are based on a node-to-surface master-slave contact formulation (Fig. 5a). In the normal direction, the contact stress σ is computed by means of the Lagrange multiplier method in compression and the linear elastic relationship $\sigma = K_{nn}u$ in tension (valid until the tensile strength f_t is reached), where K_{nn} is the cohesive stiffness in normal direction and u is the normal displacement (Fig. 5b). In the shear direction, the tangential slip δ is linearly related to the contact shear stress τ (i.e. $\tau = K_{ss}\delta$) where K_{ss} is the cohesive stiffness in shear. This relation is valid until the contact shear stress equals the shear strength f_s (Fig. 5c), which is assumed to be dependent on the contact stress $f_s(\sigma) = -\tan\phi\,\sigma + c$, where c is the cohesion and $\tan\phi$ is the initial friction of the shear response. Therefore, contact failure is supposed when the contact stresses at a point intersects a Mohr-Coulomb failure surface with tension cut-off. This criterion, implemented through an automatic subroutine ad-hoc written by the authors, can be expressed as $\max\left\{\frac{\langle\sigma\rangle}{f_t}, \frac{\tau}{f_s(\sigma)}\right\} = 1$, where the symbol $\langle x\rangle = (|x| + x)/2$ denotes the Macaulay bracket function, highlighting that masonry crushing is not accounted for in the contact response.

The maximum value of the stress in the post-peak regime, in a contact point, is described by the relationships:

$$\sigma = (1 - D)f_t, \qquad \tau = (1 - D)f_s(\sigma) + D\mu\langle-\sigma\rangle \tag{5}$$

where the degradation scalar variable D is defined as:

$$D = \begin{cases} 0, & \text{with } u \le u_0 \text{ and } \delta \le \delta_0 \\ \max\begin{cases} \dfrac{u_{MAX} - u_0}{u_k - u_0}, & \text{with } u_0 < u < u_k \\ \dfrac{\delta_{MAX} - \delta_0}{\delta_k - \delta_0}, & \text{with } \delta_0 < \delta < \delta_k \end{cases} \\ 1, & \text{with } u \ge u_k \text{ or } \delta \ge \delta_k \end{cases}, \tag{6}$$

being μ the residual friction (which is assumed in this paper equal to the initial friction $\tan\phi$, for simplicity), u_0 and δ_0 the separation and the slip at the limit of the linear elastic behaviour in tension and shear, respectively, u_{MAX} and δ_{MAX} the maximum separation and the maximum slip ever experienced by the contact point, respectively, u_k and δ_k the ultimate separation and the ultimate slip of the cohesive behaviour, respectively (Fig. 5). Particularly, in this research the value of u_k is assumed to obtain a prescribed value of fracture energy in tension G_t. Accordingly, it is also assumed $c = f_t$ and $u_k = \delta_k$ for simplicity.

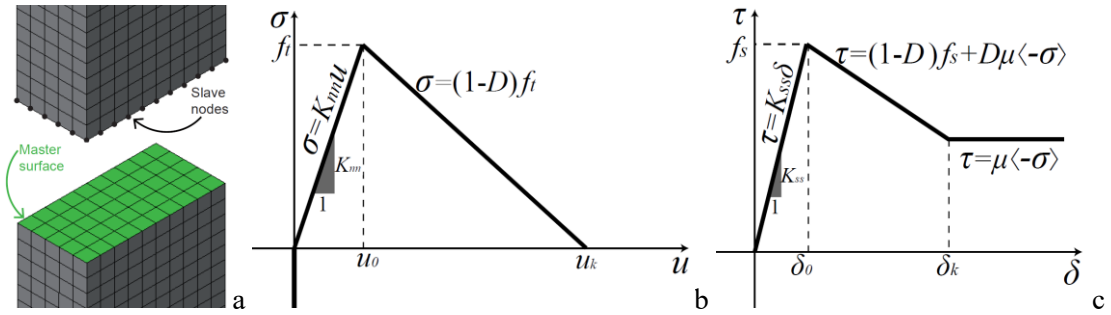

Fig. 5 – Contact-based interfaces: (a) node-to-surface contact definition, (b) tensile cohesive and (c) shear cohesive-frictional contact responses.

4.3 Some remarks

In this subsection, some remarks on the numerical modelling approaches (upper bound limit analysis, CDP and CONT) utilized in this research are provided. Particularly, the three modelling approaches show substantial differences which is herein worth to highlight.

On the one hand, upper and lower bound limit analysis permits to thoroughly bracketing the exact collapse load and mechanism for a perfectly plastic structure. On the other hand, CDP and CONT accounts for the quasi-brittle structural response, which is concentrated in the strips or interfaces. Therefore, they allow the degradation of cohesion, which is not supposed in limit analysis frameworks.

Masonry typically exhibits rather high values of friction angle (for historic masonry it generally varies from 22° to 30°). In a plasticity framework, by assuming valid the normality condition (and so assuming an associative flow rule and a Mohr-Coulomb failure surface, as in the limit analysis framework for masonry [50, 40]) high values of dilatancy are supposed, whose effects are, however, typically considered negligible. Conversely, a nonassociated plastic flow rule is supposed in the plastic damage constitutive law (CDP), where a dilatancy angle can be specified (lower than the friction angle). Even, in the contact-based interfaces (CONT) no dilatant behaviour is supposed.

Failure in compression (i.e. crushing) is supposed in the upper bound limit analysis model implemented and in the CDP model, which implements compressive softening through a damage scalar variable in compression. Conversely, no crushing is supposed in the contact-based cohesive-frictional interfaces herein adopted, although compressive failure could be accounted for in the constitutive law of the 3D solid FEs as carried out in [20].

Even though the substantial differences highlighted between the three modelling approaches here considered, they are commonly used for the numerical analysis of masonry structures [40, 41, 42, 36, 45].

5 Preliminary and parametric analyses

Some preliminary and parametric analyses are here carried out to assess the effectiveness of the incremental-iterative evolutive analysis approaches (CDP and CONT). The geometry of the benchmark of the collapse mechanism (which ideally comes from the outcomes of adaptive limit analysis) is shown in Fig. 4. The benchmark, whose overall dimension are $15 \times 16 \times 1.35$ m, is horizontally loaded with a uniform load distribution in the upper geometrical portion only. Examples of deformed contour plots (for both CDP and CONT) are depicted in Fig. 4. The mechanical properties used for the preliminary benchmark are collected in Table 2. In this subsection and in the following, hexahedral and tetrahedral FEs are considered with linear shape functions.

Table 2. Mechanical parameters used in the simulations.

	Preliminary benchmark	S. Coppito church	Two-way bending panel
Compressive strength f_c [N/m^2]	2.00	2.00	8.00
Tensile strength f_t [N/m^2]	0 – 0.2	0 – 0.05	0 – 0.32
Cohesion c [N/m^2]	f_t	f_t	f_t
Friction angle ϕ [\]	30°	30°	30°
Compressive fracture energy G_c [N/m]	1000	1000	4000
Tensile fracture energy G_t [N/m]	200	0 – 400	0 – 400
Young's modulus E [N/m^2]	2500	2500	14000
Poisson's coefficient υ [\]	0.2	0.2	0.2
Material density w [kg/m^3]	1850	1850	1850
Contact cohesive stiffness $K_{nn} = K_{ss}$ [N/m^3]	10^{10}	10^{10}	10^{11}

Firstly, the influence of the height of the strip has been investigated for the CDP approach (Fig. 6). According to the results (in terms of force-displacement curves) and the Authors' experience, a height of the strip comprised in between the 18.5% and the 25% of the thickness of the wall appears the best compromise (Fig. 6). Indeed, in order to keep the nonlinear hexahedral FEs of the strip with a reasonable aspect ratio (Fig. 6) and to prevent a too refined discretization, the height of the strip should not exceed the 25% of the thickness, and it should not be thinner than the 18.5% of the thickness. In the analyses collected in Fig. 6, a discretization with four FEs in the thickness is considered (Fig. 7). It should be pointed out that, rigorously, the strip should be barycentric on the crack of the collapse mechanism (from limit analysis). In cases alike the benchmark where the crack intercepts an opening, however, the strip unlikely can be barycentric (e.g. a nonlinear lintel would show damage even for dead load), and so the height of the strip could also alter the lever arm of the horizonal resultant (Fig. 6).

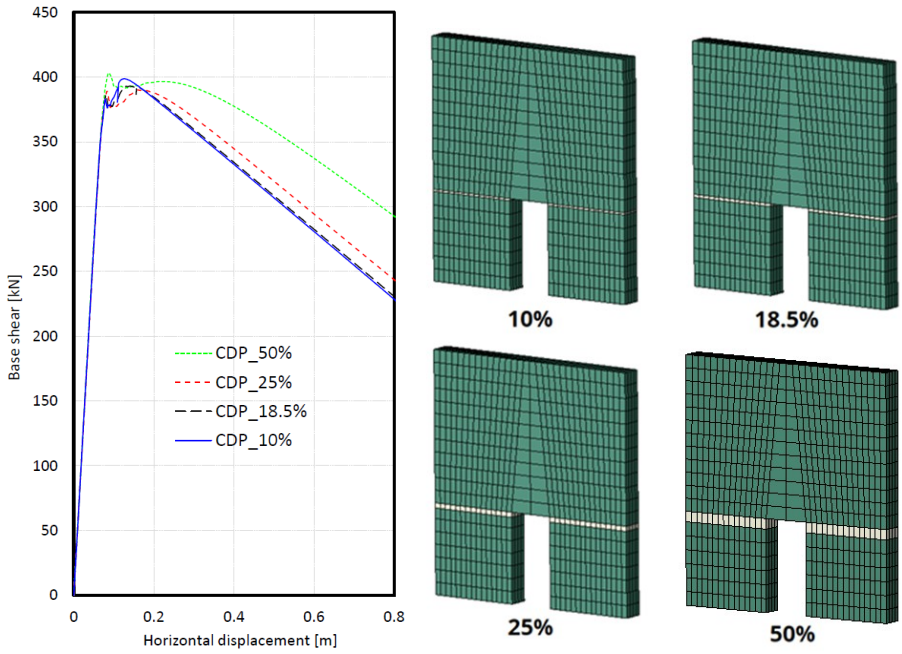

Fig. 6 – Influence of the height of the strip (CDP). The height of the strip is considered as a thickness percentage.

Secondly, the influence of the through-thickness discretization (i.e. the number of FEs in the thickness of the wall) is shown in Fig. 7 for the CDP approach. A height of the strip equal to the 18.5% of the thickness has been assumed (Fig. 6). Then, various meshes with an increasing number of elements along the thickness (as the collapse process involves out-of-plane overturning) have been tested, keeping a suitable aspect ratio in the elements. As a result, three hexahedral linear FEs in the through-thickness discretization appear sufficient to guarantee a reliable solution (Fig. 7). This consideration appears valid for structures subjected mainly to simple bending, as the benchmark analysed. When the plastic damaging strip is subjected to more complex stress states, further considerations should be contemplated (see Appendix A for torque and compression).

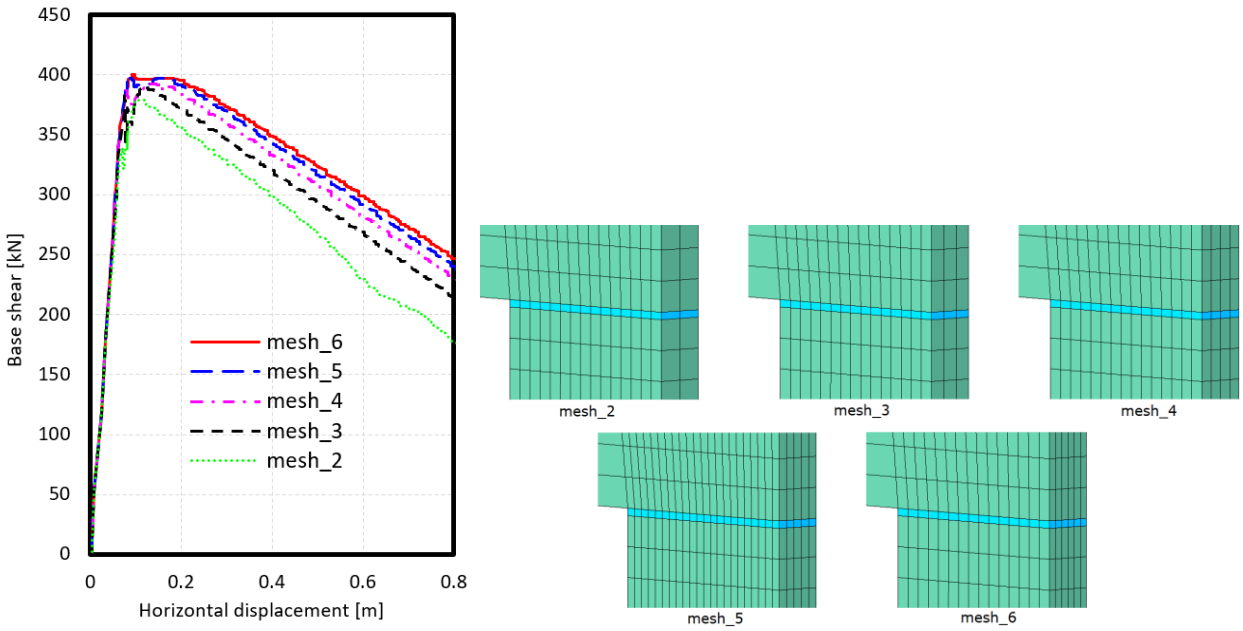

Fig. 7 – Influence of the through-thickness discretization (CDP). The notation mesh_*n* referrers to *n* as the number of FEs in the through-thickness discretization.

The influence of the through-thickness discretization is also investigated for the CONT approach (Fig. 8), as the node-to-surface contact formulation is adopted (and, so, the number of nodes in the slave face could have a role in the structural response). As can be noted in Fig. 8, the REF discretization (which shows at least four through-thickness nodes) appears the best compromise between accuracy and computational effort, and it is used in the following simulations.

As expected, the base shear becomes null, after the softening phase, for horizontal displacements generally greater than the thickness of the wall (see the graph of Fig. 8). This outcome is mainly due to the deformability of the geometrical portions, which are, conversely, considered rigid in nonlinear kinematic analyses [13].

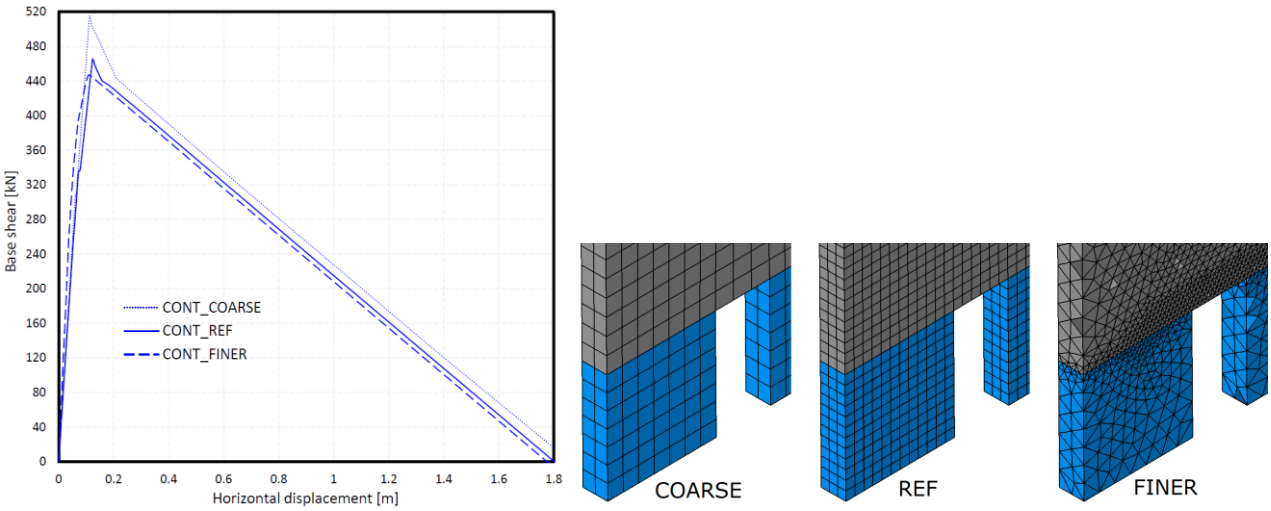

Fig. 8 – Influence of the through-thickness discretization (CONT).

The influence of load distribution on the force-displacement curves is highlighted in Fig. 9a. Rigorously, by changing the load distribution in the procedure proposed in Fig. 1, the adaptive limit analysis outcomes (e.g. collapse mechanisms) would, in general, change. Despite the load distribution changes, the collapse mechanism is kept the same (Fig. 9a) to let the reader notice the increment of base shear and displacement capacity (for both CDP and CONT approaches) that can be reached when the structure is wholly-forced (WF). This example further highlights the importance of utilizing in the CDP and CONT approaches the same loading conditions and the collapse mechanism considered and experienced in adaptive limit analysis. This key aspect is the core of the numerical procedure proposed in Fig. 1.

Fig. 9b shows the results of a parametric analysis regarding the influence of cohesion on force-displacement curves. In all the analyses, a constant value of fracture energy in tension $G_t = 200N/m$ has been considered (Table 2), except for the cases "CONT_0MPa" and "Analytical" where null cohesion and, so, null fracture energy in tension have been considered. As can be noted in Fig. 9, CDP outcomes show lower peak loads rather than CONT outcomes (typically between 10% and 20%). A no-tension model has been supposed in the CONT approach ("CONT_0MPa", where only friction has been considered in the contact-based interfaces), whereas a case with a very small value of tensile strength "CDP_0.01MPa" has been supposed in the CDP framework. This assumption of non-null tensile strength has been undertaken given that a 3D elastic isotropic no-tension continuum would collapse even under dead load. It has to be highlighted that convergence becomes problematic for very small values of tensile strength (Fig. 9b). The difference in peak loads between null (and almost-null) tensile strength and $f_t = 0.1$MPa appears greater in CDP rather than CONT, while it is greater in CONT rather than CDP between 0.1 and 0.2 MPa (Fig. 9b).

By comparing these results with an analytical solution based on the Heyman's hypotheses [4] (i.e. rigid bodies with no-slipping no-tension interfaces), the analytical collapse load appears slightly greater than the "CONT_0MPa" case, alike to the "CONT_0.1MPa" case and lower than the "CONT_0.2MPa" case, whereas all the CDP peak loads (even the one with $f_t = 0.2$MPa) are sensibly lower than the analytical solution (Fig. 9b).

In general, CDP and CONT solutions, which account for the deformability of the geometrical portions, give more conservative results (i.e. lower peak loads) with respect to Heyman-based analytical solutions. Moreover, CDP and CONT are also able to describe the force-displacement evolution of the collapse mechanism. Therefore, CDP and CONT appears, from these preliminary analyses, effective tools for the force-displacement description of collapse mechanism in masonry structures.

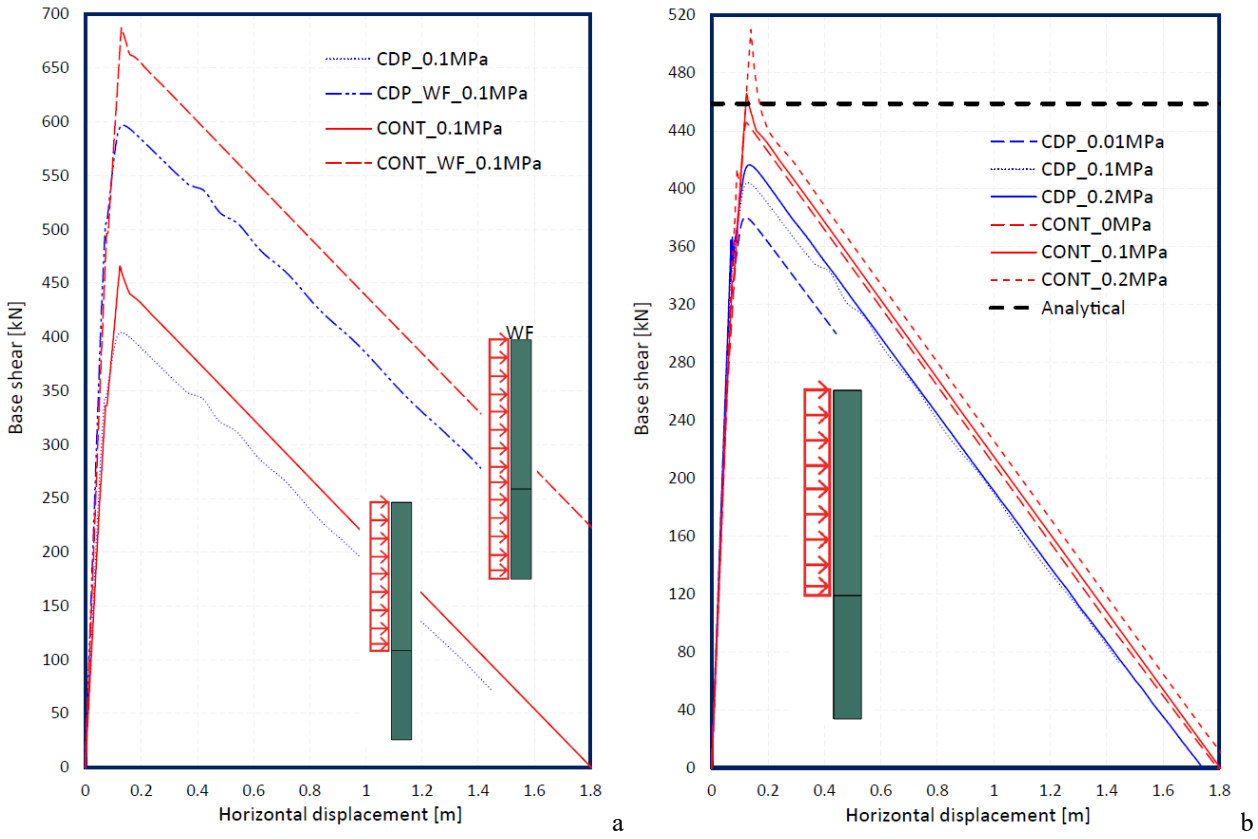

Fig. 9 – Parametric analyses: (a) influence of the load distribution and (b) influence of the cohesion.

6 Structural examples

Two structural examples are shown and discussed in this section. The first one, i.e. the façade of the S. Pietro in Coppito church, substantially consists in a masonry wall (with a complex geometry) subjected to one-way bending [41, 55]. The second one is a well-known masonry wall subjected to out-of-plane two-way bending, already analysed experimentally in [56] and numerically in [50, 57, 58, 41].

In this section, the mechanical properties have been assumed as much as consistent with the ones used in limit analysis [41] in order to provide coherent outcomes and comments (Table 2). Accordingly, the values of tensile strength, cohesion and friction angle for CONT and tensile and compressive strengths for CDP have been adopted according to the ones used in limit analysis. Indeed, different mechanical properties in limit analysis could lead, in general, to different collapse mechanisms, as already investigated in [41].

6.1 Façade of the S. Pietro in Coppito church

The church of San Pietro di Coppito in L'Aquila dates back to the 13th century, and it has been gradually transformed up to the 19th century and then restored to its initial appearance in 1969-1972. The façade of the church and its geometry, characterized by complex openings of circular and semi-circular shapes, are shown in Fig. 1. The NURBS description of the façade has been found particularly facilitated, as the NURBS description allows for a precise representation of openings of randomly complex geometries (Fig. 10). The loading conditions applied (non-uniform horizontal load), and the collapse mechanism resulted from adaptive limit analysis [41] are shown in Fig. 10. In this example, an initial population of 20 individuals has been chosen in the genetic algorithm and 10 generations have been needed to reach the optimal solution [41]. As can be noted in Fig. 10, the collapse mechanism appears quite complex. Both CDP and CONT approaches have been utilized for the force-displacement description of the collapse mechanism depicted in Fig. 10, see Fig. 1. The adopted mechanical parameters (Table 2) have been mainly taken from [41, 59]. The CDP and CONT meshes for the façade of the S. Pietro in Coppito church have been built following the indications given in Section 5.

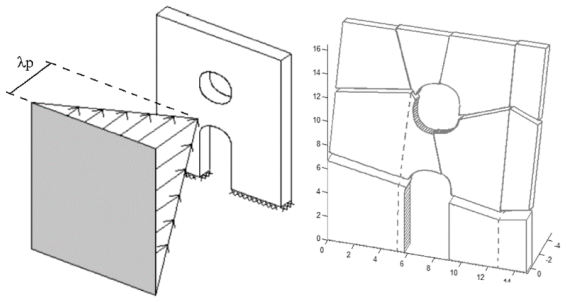

Fig. 10 – Geometry, loading conditions and collapse mechanism, from [41].

Given that the value of fracture energy in tension G_t was not available in previous literature [41], it has been parametrically assumed to vary between 0 and 400 N/m (typical values of G_t in masonry are comprised between 100 and 400 N/m), as shown in Fig. 11 in terms of force-displacement curves. The displacement time-history has been recorded on the top-right node of the structure (Fig. 10), i.e. where the horizontal load distribution shows the peak (Fig. 10). A no tension contact-based solution "CONT_no-tension" has been considered for the sake of comparison. It has to be pointed out that no convergence problems have been experienced in "CONT_no-tension" as in this case the cohesive contact behaviour has been deactivated and, so, a simple contact behaviour with friction has been implemented. Interestingly, the no tension CONT peak load is greater than the CDP with G_t =100 N/m. Indeed, also in this case CDP peak loads are systematically lower than CONT ones (e.g. "CONT_Gt=50 N/m" and "CDP_Gt=400 N/m" show akin peak loads). By inspecting Fig. 11, considerable variations of G_t lead to small variations in the peak loads and in the post-peak

response. Basically, the post-peak response (i.e. the softening regime) is not sensibly influenced by the values of G_t, and both CDP and CONT show similar behaviours.

The reference solution collected in Fig. 11 ("Limit analysis") comes from adaptive limit analysis [41], which considers, differently from the reference solution in Fig. 9b, non-zero cohesion (0.05 MPa). In this case, even though the CDP solutions seem to underestimate the peak load, CONT solutions with different values of G_t give peak loads ranging around the reference solution. In particular, the reference peak load is particularly well represented by the solution contact-based solution with G_t =100 N/m.

Fig. 12 shows the failure modes of the S. Pietro in Coppito church façade for the CDP (Fig. 12a) and CONT (Fig. 12b) approaches, for the case with G_t = 400 N/m. Even though failure modes are somehow forced on the structure, it is interesting to notice that substantially each strip/interface experiences damage in the ultimate condition (Fig. 12). Fig. 12 also shows the damage contour plots in correspondence of peak load for CDP (Fig. 12a left) and CONT (Fig. 12b left). Interestingly, the main sub-horizontal crack in the lower part of the structure shows different damage degrees in the two modelling approaches. Particularly, the damage level in this crack extends more through-thickness in CDP (Fig. 12a left) than in CONT (Fig. 12b left), in agreement with the lower peak load recorded in CDP with respect to CONT (Fig. 11). One reason of this outcome can be addressed to the excursion in the nonlinear regime of the compressed part of the CDP strip, which is already slightly recorded in correspondence of the peak load.

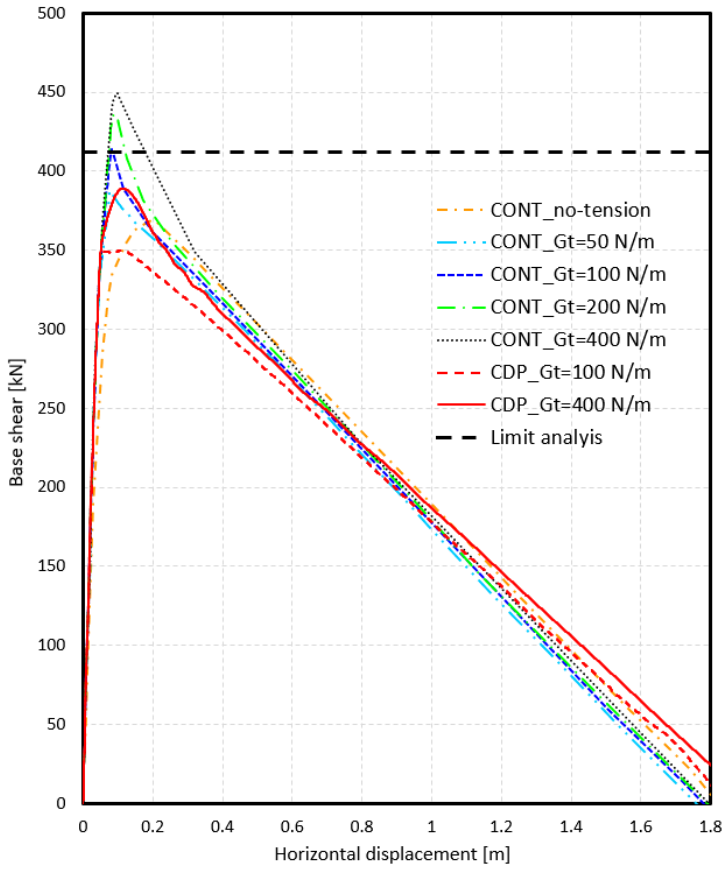

Fig. 11 – Force-displacement curves for the S. Pietro in Coppito church façade.

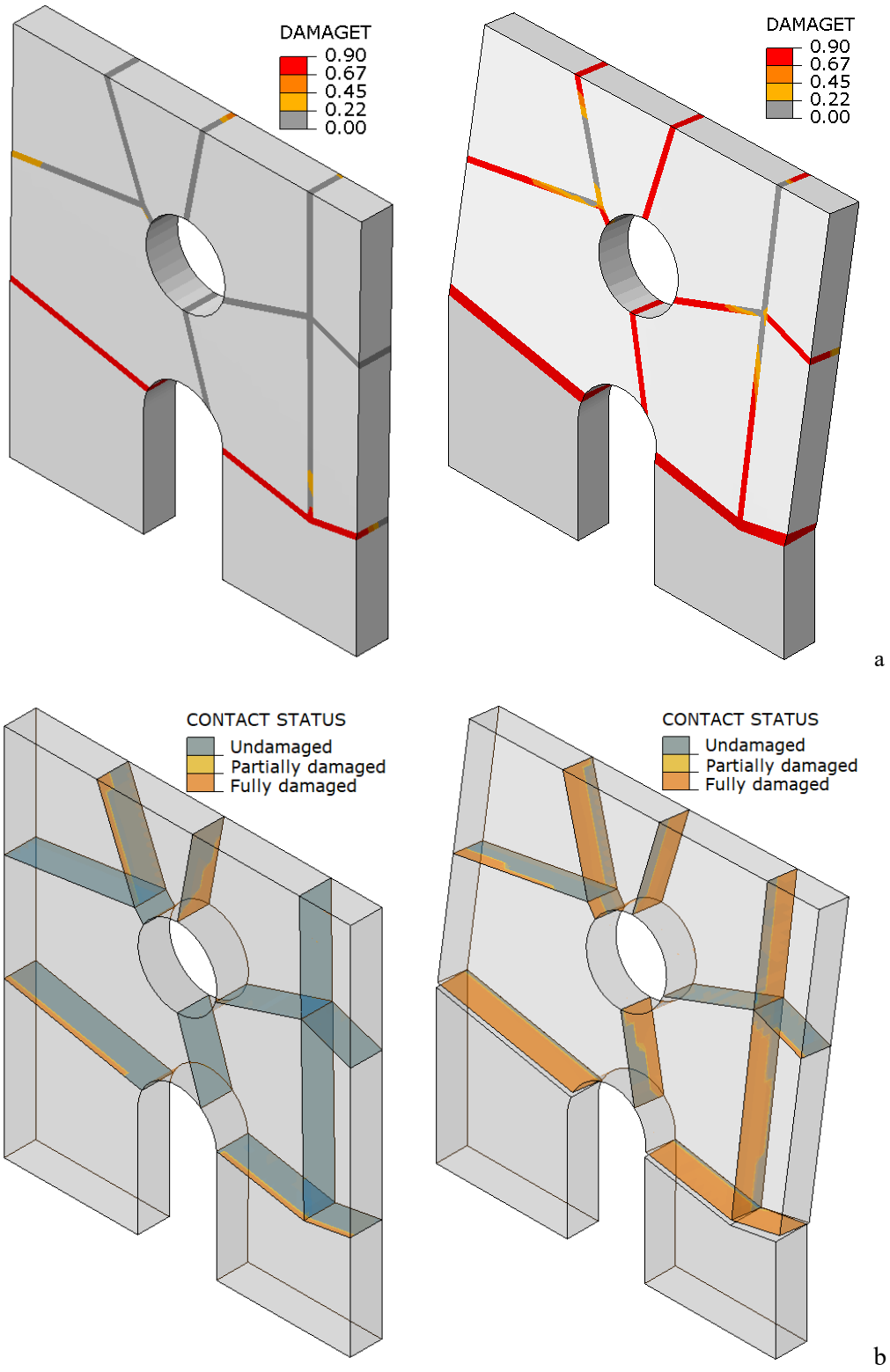

Fig. 12 – S. Pietro in Coppito church façade damage contour plots for the case with $G_t = 400$ N/m: (a) CDP tensile damage contour plots in correspondence of peak load (left) and in ultimate condition (right), and (b) CONT contact status contour plots for plots in correspondence of peak load (left) and in ultimate condition (right).

6.2 Masonry panel in two-way bending

Experimental tests on solid clay panels ($5615 \times 2475 \times 102$ mm) with and without openings were performed in [56]. Only the panels without openings (SB01 and SB05) are considered in this subsection. The panels were built in stretcher bond between two stiff abutments with the vertical edges simply supported (allowing the in-plane displacements) and the top edge free. The panels were loaded by airbags until failure. During the tests, the air pressure and the displacement for the middle point of the free edge was recorded. Both CDP and CONT approaches have been utilized for the force-displacement description of the collapse mechanism from adaptive limit analysis in [41]. In adaptive limit analysis, an initial population of 20 individuals has been chosen and 40 generations have been needed to reach the optimal solution [41]. The adopted mechanical parameters for the panel, shown in Table 2, have been taken from the literature [56, 41, 58, 50]. The CDP and CONT meshes for masonry panel in two-way bending have been built following the indications given in Section 5.

The force-displacement curves for the masonry panel in two-way bending obtained with CDP and CONT with various values of G_t are collected in Fig. 13. As can be noted, the influence of the value of G_t is much more significant than the previous case (Section 6.1). Indeed, by passing from a value of 100 N/m to 400 N/m the collapse load increases of about 50% for both approaches (CDP and CONT). Once again, the CDP peak loads are systematically lower than CONT ones. Even, the no-tension case (so with contact-based frictional interfaces) shows a peak load which is about 10 times lower than the case with G_t =100 N/m. This outcome, observed on a masonry panel in two-way bending, highlights a substantial difference from the previous case which mainly shows simple bending.

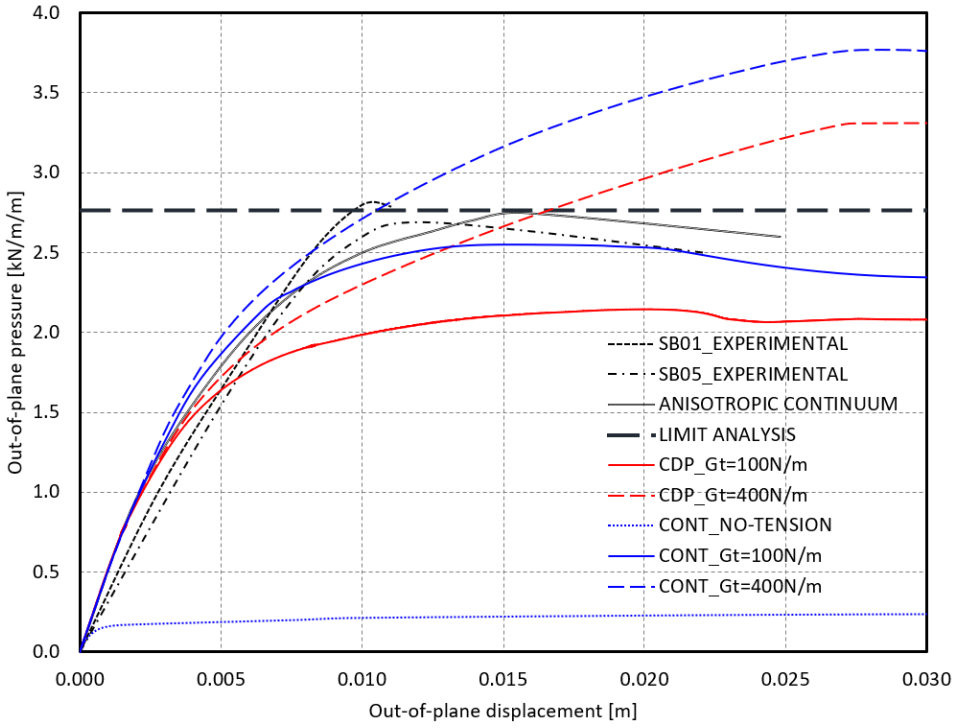

Fig. 13 – Force-displacement curves for the panel in two-way bending.

The force-displacement curves obtained following the proposed procedure are compared in Fig. 13 with the experimental curves (from [56]), an anisotropic continuum solution (from [58]), and a limit analysis solution (from [41]). As can be noted, the peak loads of the reference solutions are comprised in between the ones obtained with CDP and CONT with the border values of G_t (100 – 400 N/m). However, the CDP solution with G_t =100 N/m appears to sensibly underestimate the actual collapse load of the structure, while the CONT solution, although characterized by a lower peak load with respect to the actual one, appears closer to the experimental outcomes and to the other numerical solutions. It could be also noted in Fig. 13 that the CDP and

CONT solutions are slightly stiffer than the experimental ones, although the same value of Young's modulus suggested in [58] has been adopted in both approaches (and, indeed, the elastic branch is very close to the one predicted in [58]. Finally, it has to be noted that the curves (CDP and CONT) with the value G_t =100 N/m show a force-displacement behaviour, characterized by an elastic branch, a peak load and a softening regime with a slow decrease of the load, which can be considered reasonably in agreement with the "SB05" experimental curve [56] and the numerical curve obtained in [58].

The collapse mechanism of the masonry panel computed by adaptive limit analysis is sketched in Fig. 14a (from [41]), while the deformed contour plots for CDP and CONT are shown in Fig. 14b and Fig. 14c, respectively. Fig. 14b also shows the conforming mesh adopted in the CDP approach, which resulted quite refined aiming at having at least three through-thickness FEs. Even though failure modes are somehow forced on the structure, it is interesting to notice also in this case that substantially each interface clearly experienced failure (Fig. 14c), as well as each strip exhibited damage (as evidenced in Fig. 15 for both tensile and compressive damage).

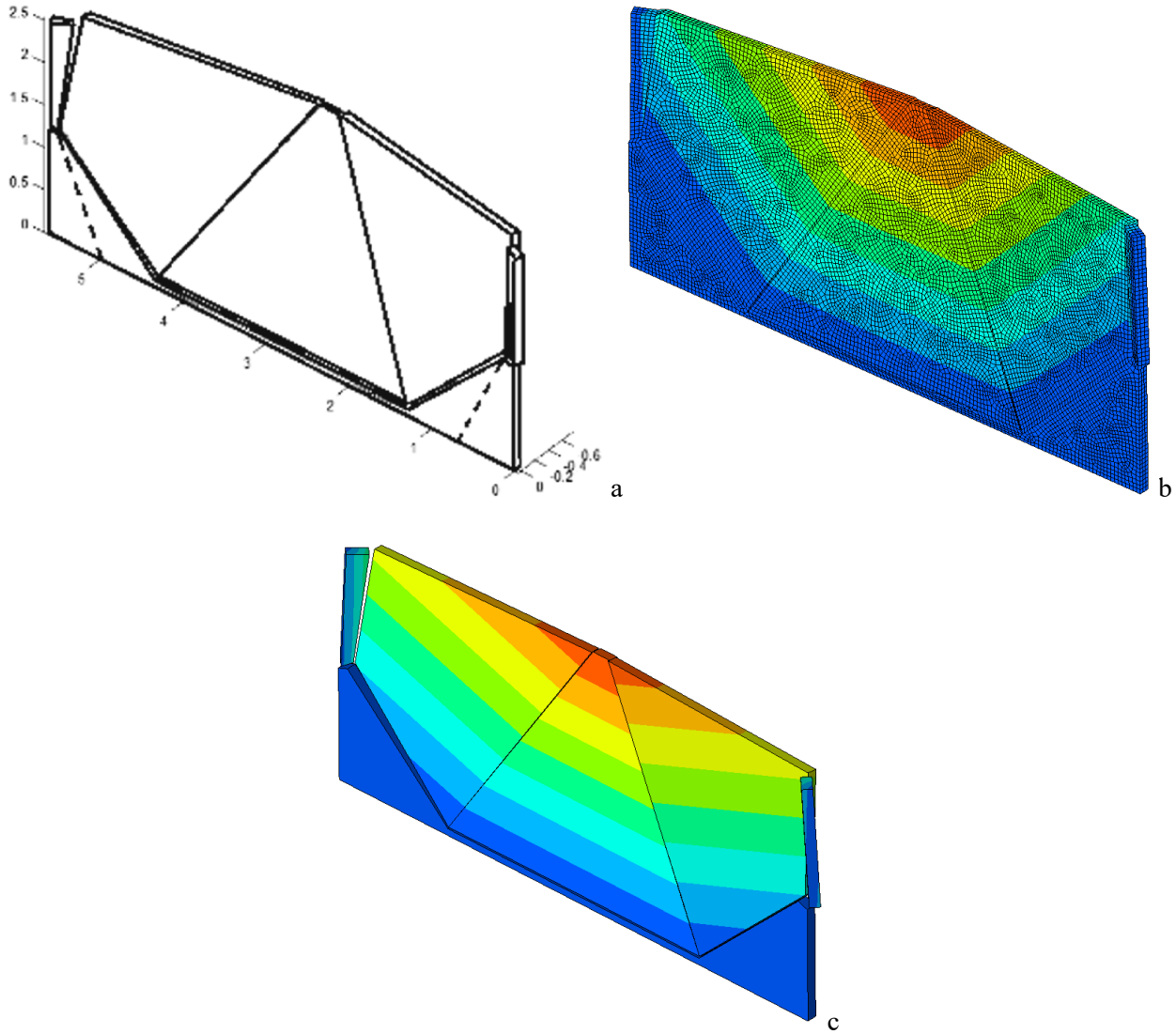

Fig. 14 – Failure modes for the panel in 2-way bending: (a) adaptive limit analysis, (b) plastic-damaging strips, (c) contact-based interfaces.

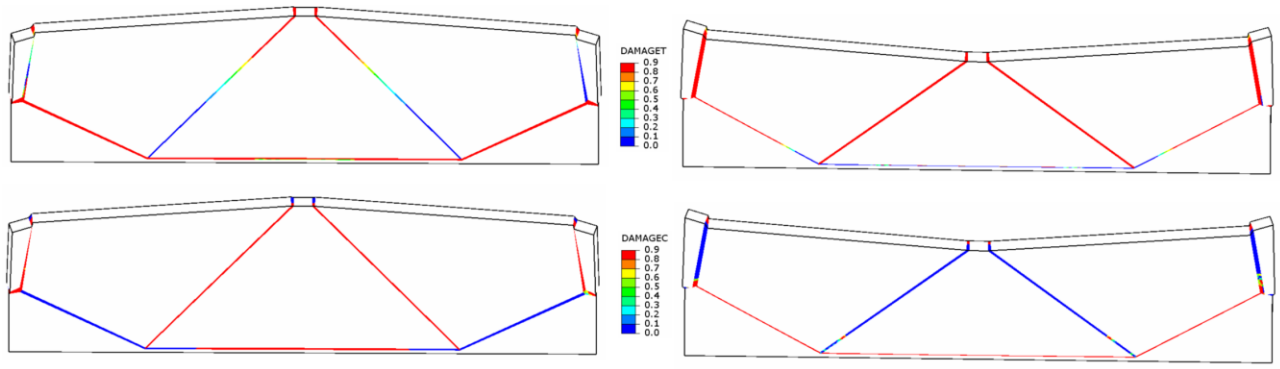

Fig. 15 – Tensile (top) and compressive (bottom) damage contour plots (CDP).

6.3 Computational effort

Given the substantially positive results previously shown, the comparison of the computational effort required in the numerical simulations for the different numerical approaches could be particularly interesting. To this aim, the computational effort needed in the numerical simulations is collected in Table 3 for the two structural examples analysed in Section 6. As can be noted, the use of contact-based interfaces (CONT) appears more computationally efficient rather than the use of plastic damaging strips (CDP), see Table 3. Particularly, the computational effort between CONT and CDP increases by passing from the façade of the S. Pietro in Coppito church (simple bending) to the masonry panel in two-way bending, also due to the small thickness which characterizes the masonry panel (Section 6.2) and leads to a considerably fine mesh for the CDP case (Fig. 14b).

Conversely, it is worth noting that is not possible to provide a precise computational burden for the adaptive limit analysis. As a matter of fact, such quantity depends on the parameters adopted in the GA, the most important being the population size. Furthermore, the number of iterations required by the GA to converge to an optimal solution depends on the individuals generated at the initial population, so two runs on the same example with the same GA parameters and mesh refinement may require different computational times. In this context, it may be pointed out that in the majority of the cases, for the examples analyzed in the paper, the converged solution was reached -assuming an initial population of 40 individuals- within 3 minutes on a PC equipped with 8Gb RAM and CPU Intel Core i7 under Matlab (Table 3).

Table 3. Computational effort required in the numerical simulations.

	Definition of the collapse mechanism*	Force-displacement description of the collapse mechanism** (for the cases with Gt=100N/m)	
	Adaptive NURBS-based limit analysis	Plastic damaging strips (CDP)(hh:mm:ss)	Contact-based interfaces (CONT) (hh:mm:ss)
Façade of the S. Pietro in Coppito church	<3 minutes	01:09:22	00:12:33
Masonry panel in two-way bending	<3 minutes	03:51:01	00:21:25
* performed on a PC equipped with 8Gb RAM and CPU Intel Core i7 under Matlab. Computational time dependent upon the GA parameters adopted. Average processing times for populations smaller than 40 individuals. ** performed on a commercial laptop equipped with a processor Intel®Core™ i7-6500U CPU @ 2.50 GHz and 16 GB RAM.			

7 Conclusions

In this paper, a novel numerical procedure has been proposed for the force-displacement description of out-of-plane collapse in masonry structures, representing one first attempt to couple limit analysis-based solutions to displacement-based evolutive analysis strategies.

In this way, the limitations of limit analysis-based solutions, which cannot contemplate the force-displacement description of collapse mechanisms and, so, they cannot be used in displacement-based seismic assessment procedures (e.g. pushover analysis), and the limitations of displacement-based evolutive analysis strategies (e.g. block-based and anisotropic continuum approaches), which are typically computationally demanding, are overcame.

Particularly, adaptive NURBS-based limit analysis is firstly adopted to compute the collapse mechanism that the structure (of any geometrical complexity) experiences for a given loading condition. Then, the geometry of the collapse mechanism is imported in incremental-iterative step-by-step evolutive analysis frameworks to perform pushover analysis.

Two numerical modelling approaches, lumping the nonlinearities into tight zones located in correspondence of the cracks defined in the collapse mechanism, have been developed and tested.

Plastic damaging strips governed by a standard nonlinear continuum constitutive law (CDP) and non-standard zero-thickness contact-based interfaces governed by a cohesive-frictional contact behaviour (CONT) have been implemented, tested and compared for a number of meaningful structural examples. Particularly, it has been systematically observed slightly lower peak loads in plastic damaging strips than in contact-based interfaces. One reason of this outcome can be addressed to the excursion in the nonlinear regime which can occur in the compressed part of plastic damaging strips, while the contact-based interfaces do not account for crushing.

The procedure appeared significantly appealing and reliable for the force-displacement description of collapse in masonry structures. Contextually, the use of cohesive-frictional contact-based interfaces has been found to be especially efficient. In particular, contact-based interfaces appeared to be preferable than plastic damaging strips, given their more limited computational effort and the fully automatic model geometrical definition. In addition, the capability to directly define the shear behaviour of the contact-based interfaces appears another positive feature, whereas in plastic damaging strips the shear behaviour is indirectly described from tensile and compressive behaviours.

It should be highlighted that the numerical procedure proposed herein works effectively for out-of-plane collapse mechanisms only. The applicability of this numerical procedure for in-plane loaded masonry structures is currently under investigation by the authors, through the use of nonlinearities in the macro-blocks to account for masonry crushing as well.

To conclude, it has to be pointed out that the numerical procedure proposed in this research appears particularly appealing also for large-scale heritage structures, i.e. characterized by a significant thickness of the walls. Indeed, the mesh size to be adopted in the models has been found to be related to the wall thickness, and, hence, larger thicknesses would lead to larger mesh sizes. Therefore, this allows to keep the computations affordable even when dealing with monumental buildings.

ACKNOWLEDGEMENTS

Financial support by the Italian Ministry of Education, Universities and Research MIUR is gratefully acknowledged (PRIN2015 “Advanced mechanical modelling of new materials and structures for the solution of 2020 Horizon challenges” prot. 2015JW9NJT_018).

Appendix A

A simple benchmark ($1.0 \times 1.0 \times 4.2$m, see Fig. 16) is herein adopted to show some issues on the mesh discretization of the plastic damaging strip (height equal to 0.2m) in the CDP framework, when simultaneously subjected to compression and torsion. The mechanical properties adopted for the nonlinear blue strip (Fig. 16) are collected in Table 2 (the same of “Preliminary benchmark”), while the other parts (grey, Fig. 16) are kept linear elastic. The vertical force-displacement and torsional moment-rotation curves are collected in Fig. 16 for two mesh discretizations (coarse and fine as shown in Fig. 17). Particularly, the graphs on the right of Fig. 16 (highlighted in light blue) represent an enlargement of the very first part of the graphs on the left of Fig. 16 (small rectangles highlighted in light blue). As can be noted, the coarse mesh (Fig. 17) appears not able to properly catch the damaging phenomenon of the strip, showing an indefinite capacity to carry vertical compression and torque Fig. 16, even though the nonlinear strip of the benchmark (blue in Fig. 16) implements the plastic damage constitutive law discussed in Section 4.1. When the mesh of the nonlinear strip is further refined (Fig. 17), this issue appears resolved, and the structural response shows softening in both compression and torsion (Fig. 16). This example highlighted the need of paying particular attention on the mesh discretization of the plastic damaging strip in the CDP approach.

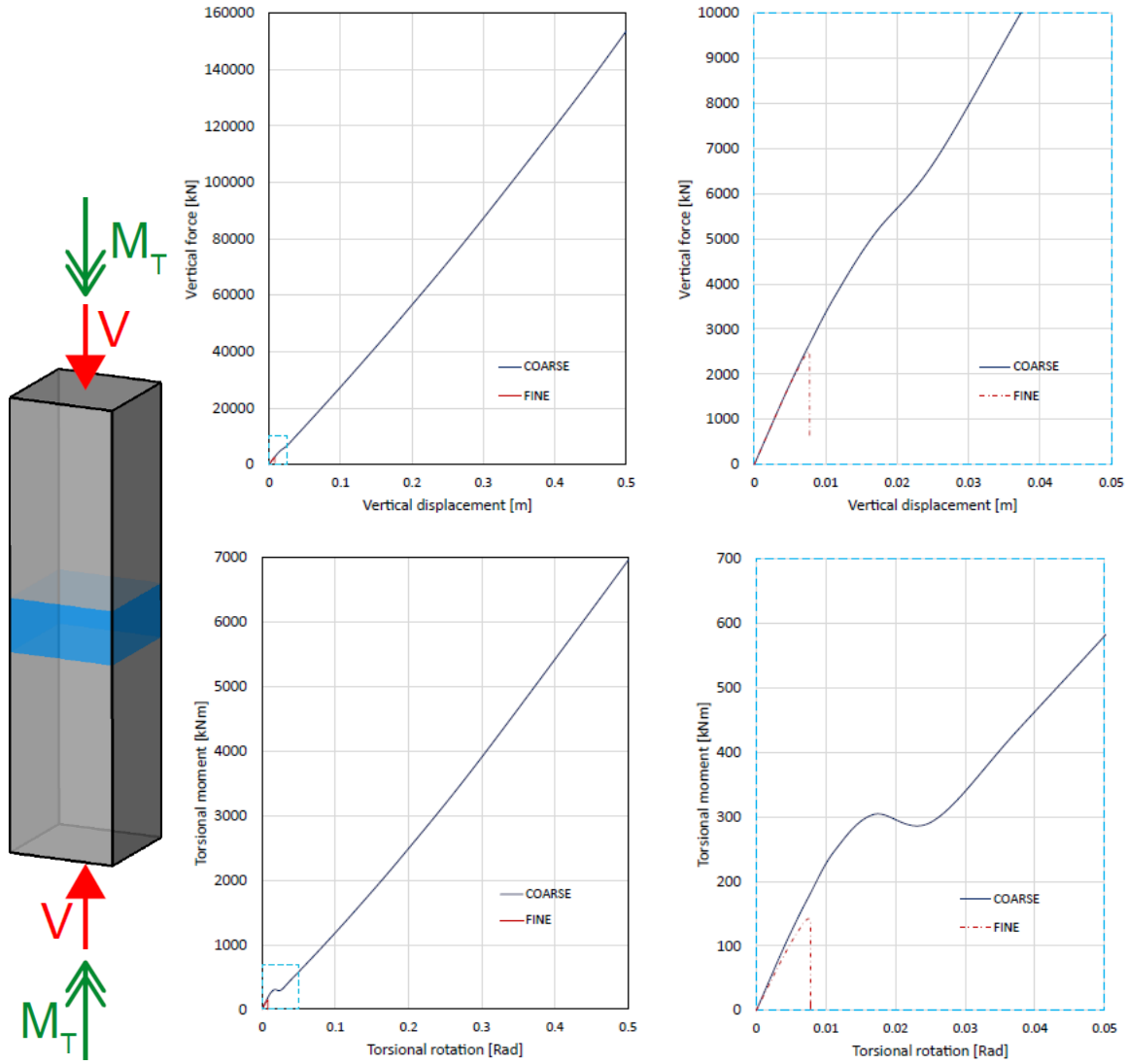

Fig. 16 – Benchmark simultaneously subjected to compression and torsion: vertical force-displacement and torsional moment-rotation curves.

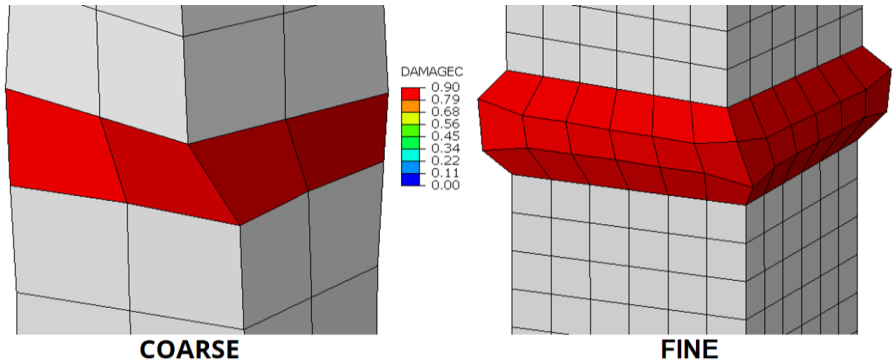

Fig. 17 – Benchmark simultaneously subjected to compression and torsion: particular of the coarse and fine meshes.

REFERENCES

[1] W. Addis, Building: 3000 years of design engineering and construction, Phaidon Press, 2007.

[2] S. Cattari, S. Degli Abbati, D. Ferretti, S. Lagomarsino, D. Ottonelli and A. Tralli, "Damage assessment of fortresses after the 2012 Emilia earthquake (Italy)," *Bulletin of Earthquake Engineering,* vol. 12, no. 5, pp. 2333-2365, 2014 doi:10.1007/s10518-013-9520-x.

[3] M. Malena, F. Portioli, R. Gagliardo, G. Tomaselli, L. Cascini and G. de Felice, "Collapse mechanism analysis of historic masonry structures subjected to lateral loads: A comparison between continuous and discrete models," *Computers & Structures,* vol. 220, pp. 14-31, 2019.

[4] J. Heyman, "The stone skeleton," *International Journal of Solids and Structures,* vol. 2, no. 2, p. 249–279, 1966.

[5] P. Block and J. Ochsendorf, "Thrust network analysis: A new methodology for three-dimensional equilibrium," *Journal of the International Association for shell and spatial structures,* vol. 48, no. 3, pp. 167-173, 2007.

[6] F. Fraternali, "A thrust network approach to the equilibrium problem of unreinforced masonry vaults via polyhedral stress functions," *Mechanics Research Communications,* vol. 37, no. 2, p. 198–204, 2010.

[7] F. Marmo and L. Rosati, "Reformulation and extension of the thrust network analysis," *Computers & Structures,* vol. 182, p. 104–118, 2017.

[8] M. Angelillo, "Static analysis of a Guastavino helical stair as a layered masonry shell," *Composite Structures,* vol. 119, p. 298–304, 2015.

[9] F. Portioli, C. Casapulla, M. Gilbert and L. Cascini, "Limit analysis of 3D masonry block structures with non-associative frictional joints using cone programming," *Computers & Structures,* vol. 143, p. 108–121, 2014.

[10] G. Milani, P. Lourenço and A. Tralli, "Homogenised Limit Analysis of Masonry Walls, Part I: Failure Surfaces," *Computers & Structures,* vol. 84, no. 3-4, p. 166–180, 2006 doi:10.1016/j.compstruc.2005.09.005.

[11] G. Milani, P. Lourenço and A. Tralli, "Homogenised Limit Analysis of Masonry Walls, Part II: Structural Examples," *Computers & Structures,* vol. 84, no. 3-4, p. 181–195, 2006 doi:10.1016/j.compstruc.2005.09.004.

[12] S. Sloan and P. Kleeman, "Upper Bound Limit Analysis Using Discontinuous Velocity Fields," *Computer Methods in Applied Mechanics and Engineering,* vol. 127, no. 1-4, p. 293–314, 1995 doi:10.1016/0045-7825(95)00868-1.

[13] M. Godio and K. Beyer, "Evaluation of force-based and displacement-based out-of-plane seismic assessment methods for unreinforced masonry walls through refined model simulations," *Earthquake Engineering & Structural Dynamics,* vol. 48, no. 4, p. 454–475, 2018.

[14] D. Baraldi and A. Cecchi, "Discrete and continuous models for static and modal analysis of out of plane loaded masonry," *Computers & Structures,* vol. 207, pp. 171-186, 2018.

[15] D. Baraldi and A. Cecchi, "Discrete Approaches for the Nonlinear Analysis of in Plane Loaded Masonry Walls: Molecular Dynamic and Static Algorithm Solutions," *European Journal of Mechanics - A/Solids,* vol. 57, p. 165–177, 2016.

[16] D. Malomo, R. Pinho and A. Penna, "Using the applied element method for modelling calcium silicate brick masonry subjected to in-plane cyclic loading," *Earthquake Engineering & Structural Dynamics,* vol. 47, no. 7, p. 1610–1630, 2018.

[17] C. Chisari, L. Macorini, C. Amadio and B. A. Izzuddin, "An inverse analysis procedure for material parameter identification of mortar joints in unreinforced masonry," *Computers & Structures,* vol. 155, p. 97–105, 2015.

[18] T. Y. Yuen, T. Deb, H. Zhang and Y. Liu, "A fracture energy based damage-plasticity interfacial constitutive law for discrete finite element modelling of masonry structures," *Computers & Structures,* vol. 220, pp. 92-113, 2019.

[19] D. Foti, V. Vacca and I. Facchini, "DEM modelling and experimental analysis of the static behavior of a dry-joints masonry cross vaults," *Construction and Building Materials,* vol. 170, p. 111–120, 2018.

[20] A. M. D'Altri, S. de Miranda, G. Castellazzi and V. Sarhosis, "A 3D Detailed Micro-Model for the In-Plane and Out-Of-Plane Numerical Analysis of Masonry Panels," *Computers & Structures,* vol. 206, pp. 18-30, 2018.

[21] M. Petracca, L. Pelà, R. Rossi, S. Zaghi, G. Camata and E. Spacone, "Micro-Scale Continuous and Discrete Numerical Models for Nonlinear Analysis of Masonry Shear Walls," *Construction and Building Materials,* vol. 149, p. 296–314, 2017.

[22] J. Scacco, B. Ghiassi, G. Milani and P. B. Lourenço, "A fast modelling approach for numerical analysis of unreinforced and FRCM reinforced masonry walls under out-of-plane loading," *Composites Part B: Engineering,* vol. 180, p. 107553, 2020.

[23] K. F. Abdulla, L. S. Cunningham and M. Gillie, "Simulating masonry wall behaviour using a simplified micro-model approach," *Engineering Structures,* vol. 151, p. 349–365, 2017.

[24] S. Tiberti and G. Milani, "2D pixel homogenized limit analysis of non-periodic masonry walls," *Computers & Structures,* vol. 219, pp. 16-57, 2019.

[25] P. B. Lourenço, J. G. Rots and J. Blaauwendraad, "Continuum Model for Masonry: Parameter Estimation and Validation," *Journal of Structural Engineering,* vol. 124, no. 6, p. 642–652, 1998.

[26] L. Berto, A. Saetta, R. Scotta and R. Vitaliani, "An Orthotropic Damage Model for Masonry Structures," *International Journal for Numerical Methods in Engineering,* vol. 55, no. 2, p. 127–157, 2002.

[27] L. Pelà, M. Cervera and P. Roca, "An Orthotropic Damage Model for the Analysis of Masonry Structures," *Construction and Building Materials,* vol. 41, p. 957–967, 2013.

[28] B. Pantò, F. Cannizzaro, S. Caddemi and I. Caliò, " 3D macro-element modelling approach for seismic assessment of historical masonry churches," *Advances in Engineering Software,* vol. 97, p. 40–59, 2016.

[29] S. Brasile, R. Casciaro and G. Formica, "Finite Element formulation for nonlinear analysis of masonry walls," *Computers & Structures,* vol. 88, no. 3-4, p. 135–143, 2010.

[30] B. Ghiassi, M. Soltani and A. A. Tasnimi, "A simplified model for analysis of unreinforced masonry shear walls under combined axial, shear and flexural loading," *Engineering Structures,* vol. 42, p. 396–409, 2012.

[31] E. Bertolesi, G. Milani and P. B. Lourenço, "Implementation and validation of a total displacement non-linear homogenization approach for in-plane loaded masonry," *Computers & Structures,* vol. 176, p. 13–33, 2016.

[32] P. Di Re, D. Addessi and E. Sacco, "A multiscale force-based curved beam element for masonry arches," *Computers & Structures,* vol. 208, pp. 17-31, 2018.

[33] M. Petracca, L. Pelà, R. Rossi, S. Oller, G. Camata and E. Spacone, "Regularization of first order computational homogenization for multiscale analysis of masonry structures," *Computational Mechanics,* vol. 57, no. 2, pp. 257-276, 2015.

[34] S. Invernizzi, G. Lacidogna, N. E. Lozano-Ramírez and A. Carpinteri, "Structural monitoring and assessment of an ancient masonry tower," *Engineering Fracture Mechanics,* 2018 In Press.

[35] G. Bartoli, M. Betti e A. Vignoli, «A numerical study on seismic risk assessment of historic masonry towers: a case study in San Gimignano,» *Bulletin of Earthquake Engineering,* vol. 14, n. 6, p. 1475–1518, 2016.

[36] G. Milani, M. Valente and C. Alessandri, "The Narthex of the Church of the Nativity in Bethlehem: A Non-Linear Finite Element Approach to Predict the Structural Damage," *Computers & Structures,* 2017 doi:10.1016/j.compstruc.2017.03.010.

[37] S. Degli Abbati, A. M. D'Altri, D. Ottonelli, G. Castellazzi, S. Cattari, S. de Miranda and S. Lagomarsino, "Seismic assessment of interacting structural units in complex historic masonry constructions by nonlinear static analyses," *Computers & Structures,* vol. 213, pp. 51-71, 2019.

[38] M. Godio and K. Beyer, "Analytical model for the out-of-plane response of vertically spanning unreinforced masonry walls," *Earthquake Engineering & Structural Dynamics,* vol. 46, no. 15, p. 2757–2776, 2017.

[39] M. Godio and K. Beyer, "Tri-linear model for the out-of-plane seismic assessment of vertically-spanning unreinforced masonry walls," *Journal of Structural Engineering,* 2019 (In press).

[40] A. Chiozzi, G. Milani and A. Tralli, "A Genetic Algorithm NURBS-based new approach for fast kinematic limit analysis of masonry vaults," *Computers & Structures,* vol. 182, p. 187–204, 2017.

[41] A. Chiozzi, G. Milani, N. Grillanda and A. Tralli, "A fast and general upper-bound limit analysis approach for out-of-plane loaded masonry walls," *Meccanica,* vol. 53, no. 7, pp. 1875-1898, 2018.

[42] A. Chiozzi, N. Grillanda, G. Milani and A. Tralli, "UB-ALMANAC: An adaptive limit analysis NURBS-based program for the automatic assessment of partial failure mechanisms in masonry churches," *Engineering Failure Analysis,* vol. 85, p. 201–220, 2018.

[43] J. Lee and G. L. Fenves, "Plastic-Damage Model for Cyclic Loading of Concrete Structures," *Journal of Engineering Mechanics,* vol. 124, no. 8, p. 892–900, 1998 doi:10.1061/(asce)0733-9399(1998)124:8(892).

[44] *Abaqus®. Theory manual, Version 6.17, 2017.*

[45] A. M. D'Altri, F. Messali, J. Rots, G. Castellazzi and S. de Miranda, "A damaging block-based model for the analysis of the cyclic behaviour of full-scale masonry structures," *Engineering Fracture Mechanics,* vol. 209, pp. 423-448, 2019.

[46] N. Cavalagli, A. Kita, V. L. Castaldo, A. L. Pisello and F. Ubertini, "Hierarchical environmental risk mapping of material degradation in historic masonry buildings: An integrated approach considering climate change and structural damage," *Construction and Building Materials,* vol. 215, p. 998–1014, 2019.

[47] R. McNeel, "Rhinoceros: NURBS modelling for Windows," Robert McNeel & Associates, Seattle, 2008.

[48] L. Piegl and W. Tiller, The NURBS book, Springer Science & Business Media, 2012.

[49] P. Kennicott, "Initial Graphics Exchange Specification, IGES 5.3," U.S. Product Data Association, 1966.

[50] G. Milani, P. Lourenço and A. Tralli, "Homogenization approach for the limit analysis of out-of-plane loaded masonry walls," *Journal of structural engineering,* vol. 132, no. 10, pp. 1650-1663, 2006.

[51] G. Milani and A. Taliercio, "In-plane failure surfaces for masonry with joints of finite thickness estimated by a method of cells-type approach," *Computers & Structures,* vol. 150, pp. 34-51, 2015.

[52] G. Milani and A. Taliercio, "Limit analysis of transversally loaded masonry walls using an innovative macroscopic strength criterion," *International Journal of Solids and Structures,* vol. 81, pp. 274-293, 2016.

[53] J. F. Sturm, "Using SeDuMi 1.02, a MATLAB toolbox for optimization over symmetric cones," *Optimization methods and software,* vol. 11, no. 1-4, pp. 625-653, 1999.

[54] R. L. Haupt and S. E. Haupt, Practical Genetic Algorithms, John Wiley & Sons, Inc, 1998.

[55] G. Boscato, M. Pizzolato, S. Russo and A. Tralli, "Seismic behavior of a complex historical church in L'Aquila," *International Journal of Architectural Heritage,* vol. 8, no. 5, pp. 718-757, 2014.

[56] V. L. Chong, "The behaviour of laterally loaded masonry panels with openings," PhD dissertation, University of Plymouth, Plymouth, 1993.

[57] G. Milani, "Homogenized limit analysis of FRP-reinforced masonry walls out-of-plane loaded," *Computational Mechanics,* vol. 43, no. 5, pp. 617-639, 2009.

[58] P. B. Lourenço, "An anisotropic macro-model for masonry plates and shells: Implementation and validation," PhD Dissertation, Delft University of Technology, Delft, 1997.

[59] "Circolare 617-02/02/2009. Istruzioni per l'applicazione delle nuove norme tecniche per le costruzioni di cui al decreto ministeriale 14 Gennaio 2008".